Long-Term Reliability of Low-Carbon Integrated Electricity and Gas Systems: Impact of Alternative Gas Injection

Sheng Wang[a,b,c], Hongxun Hui[a,b*], Yi Ding[d], Yonghua Song[a,b]

[a]*State Key Laboratory of Internet of Things for Smart City, University of Macau, Macao, 999078, China*
[b]*Department of Electrical and Computer Engineering, University of Macau, Macao, 999078, China*
[c]*State Grid Suzhou City and Energy Research Institute Co Ltd, Suzhou, 215163, China*
[d]*College of Electrical Engineering, Zhejiang University, Hangzhou, 310058, China*

Abstract

Power-to-gas facilities consume surplus renewable electricity generations to produce alternative gases, such as green hydrogen and methane. They can be injected into, and transported by the gas network for further use, which is a promising way toward a low-carbon energy system. However, injecting alternative gases into the gas systems can adversely affect the gas composition and the lifespan of components (e.g., gas pipelines), and may threaten the reliability of the entire integrated electricity and gas systems (IEGS) in the long term. To address this issue, this paper proposes a long-term reliability evaluation method for IEGS with alternative gas injections. First, new reliability indices are proposed to evaluate both gas adequacy and gas interchangeability under uncertainties. Then, a multi-state reliability model of the pipeline is developed to characterize the corrosion evolution and hydrogen embrittlement in the long term. A contingency management scheme (CMS) is devised to minimize load curtailments and gas interchangeability deviations under component failures. Moreover, several reformulation techniques are tailored to convexify the original two-stage mixed-integer nonlinear CMS optimization problem. An analytical reliability evaluation method embedded with a system state reduction technique is designed to evaluate the long-term reliability of the IEGS more efficiently. Finally, the IEEE 24 bus Reliability Test System and the practical Belgium gas system are used to validate the proposed method. The numerical results show that the injection of alternative gas could jeopardize the reliability of the studied IEGS by 39.73% in the long term. However, we have observed a critical time

---

*Corresponding author
Email address:* `hongxunhui@um.edu.mo` (Hongxun Hui[a,b])

window (the 8th-9th year), in which if we conduct the inline inspection and maintenance more frequently, the reliability could be improved by up to 53.31%. These results suggest that the injection of alternative gas is beneficial, but should be carefully regulated to maintain the reliability of IEGS.

1. Introduction

With the growing concerns for low-carbon development, hydrogen has become one of the most appealing alternative gas. Blending hydrogen into the existing gas systems is the current focus in many countries to decarbonize the energy systems. For example, Energy Networks Association in the UK calls for 20% hydrogen blending into gas networks from 2023, which will save around 6 Mt/year of carbon dioxide emission [1]. As Spain's second-largest natural gas distribution company, Nortegas also plans to gradually blend hydrogen into its residential and industrial gas network [2]. Green hydrogen is usually produced by power-to-gas (PTG) facilities by consuming the surplus renewable electricity generation. The installations of PTGs, together with the existing gas-fired power plants (GPP), have intensified the interdependency of the electricity and gas systems in a bidirectional way. Therefore, the two energy systems tend to be regarded and regulated as a whole integrated electricity and gas systems (IEGS).

However, injecting alternative gases (including hydrogen, methane, and biogas) into the IEGS may jeopardize the reliabilities from the following aspects: 1) the distributed injections of alternative gases will continuously change the gas composition across the gas network. The gas appliances, which are usually designed and tested at a given gas composition, may not perform satisfactorily or reliably under an uncertain gas composition [3]; 2) the varying gas composition may change the physical characteristics of the gas mixtures (such as specific gravity, gross caloric value (GCV), etc.), and further change the gas flow pattern. When gas composition changes, some gas demands may not be supplied with sufficient gas in terms of both quantity and heat energy [4]; 3) the injected hydrogen may corrode the material of pipelines, which is also known as hydrogen embrittlement [5]. The reliability of pipelines will be jeopardized, which affects the reliability of the whole IEGS in the long term. Therefore, the long-term reliability

evaluation of IEGS with alternative gas injections is urgently required.

The reliability of IEGS with constant gas composition has been extensively studied in previous studies [6, 7]. However, when alternative gas injections and varying gas compositions are considered, most of the existing studies focus on gas composition tracking and simulation problems. The steady-state simulation method of gas systems with the distributed injections of hydrogen and upgraded biogas is developed in [8]. It validates that appropriate management of diverse gas supply sources can reduce carbon emissions. An efficient simulation method for long-distance gas transport networks with large amounts of hydrogen injection is proposed in [9]. A probabilistic multi-energy flow calculation method for IEGS with hydrogen injection is proposed in [10]. A transient analysis model for gas systems is developed in [11], which enables gas composition tracking in meshed networks with multiple distributed gas sources and intermittent hydrogen injections. The impacts of different hydrogen blending modes on the IEGS are simulated and discussed in [12]. Though these studies can simulate the operating condition and gas composition in the IEGS with alternative gas injections, they may not be able to optimize the system's condition. For example, they cannot provide quantitative corrective measures if some security constraints are violated.

Recently, some studies have been dedicated to the optimization and regulation of gas system security with alternative gas injections. For example, the impacts of distributed renewable generations on the IEGS security through PTGs are investigated in [13] and [14]. A unit commitment model for electricity systems and the optimal energy flow model for gas systems are performed separately in [15] to track and optimize the gas composition with hydrogen injections. A distributionally robust optimization model of IEGS is developed in [16] to cope with the impacts of wind power fluctuations on the gas system security. An optimal stochastic operation model of the electricity-hydrogen-transportation system with renewable energies is investigated in [17]. A chance-constrained energy and reserve joint scheduling model for wind-photovoltaic-hydrogen integrated energy system is developed in [18]. A Coordinated operation model of electricity and gas-hydrogen systems with transient gas flow conditions is proposed in [19]. However, these studies focus on the short-term secured operations of IEGS under the uncertainties of renewable generations. The long-term impacts of alternative gas injections with inherent uncertainties, such as hydrogen embrittlement,

the IEGS component failures (such as the failures of gas sources and pipelines), etc., on the reliability of IEGS, have not been investigated yet.

The long-term reliability evaluation of IEGS with alternative gas injections is challenging for the following reasons. 1) There lacks an index that can quantify the reliability of IEGS with varying gas compositions. Gas interchangeability is usually used as an index to describe whether the gas composition is acceptable for gas appliances [20]. However, under multiple uncertainties, the gas composition may also vary stochastically. The probability of the gas composition falling in the acceptable range, and the expected deviation from the acceptable range can not be quantified by using gas interchangeability or other off-the-shelf indices. 2) The impacts of various component failures, especially the different failure modes of pipelines, on the reliability of the IEGS are difficult to characterize. Some basic models are introduced in previous studies. For example, the stochastic failure process of the pipeline due to corrosion in the long-term can be modeled as the Markov process in [21], Gamma process in [22], etc. The impact of hydrogen embrittlement on the burst pressure of pipelines is quantitatively investigated in [23]. However, these pipeline corrosion models are time continuous. Directly adopting these models in the reliability evaluation of IEGS will be very time-consuming. 3) The optimal energy flow model of IEGS considering the blending of alternative gases is a highly nonlinear and mixed-integer optimization problem, for they make the originally constant physical parameters (such as specific gravity, the GCV of the gas) into variables. Though some studies have introduced sequential linear programming, polyhedral envelopes, etc., to solve the optimization problem [24], they are either not accurate enough for the reliability evaluation where the system condition changes dramatically, or not efficient enough for the reliability evaluation where the optimization problem will be solved repeatedly for numerous scenarios.

To address the above research gaps, this paper proposes a long-term reliability evaluation framework for IEGS to quantify the impacts of alternative gas injections. The contributions are summarized as:

1) A set of novel reliability indices is proposed to quantify the impacts of alternative gas injections. Derived from the Dutton diagram method, we formulate two new reliability indices: expected gas interchangeability deviation (EGID) and gas interchangeability deviation probability (GIDP). Compared with traditional deterministic security indices

such as Wobbe Index, the proposed expectation-based reliability indices can better measure the deviation of the gas mixtures from acceptable gas composition regions (AGCR) under various long-term uncertainties.

2) A multi-state reliability model of the pipeline is developed to incorporate the corrosion effect in the long term. The evolution of the corrosion process for each pipeline segment is modeled using the independent Gamma process. By using the limit state functions of multiple failure modes (including small gas leak, large gas leak, and rupture failure), the continuous Gamma process can be discretized into several states using the reliability network equivalent technique to reduce the computation burden. The impacts of hydrogen embrittlement are also modeled in the limit state functions.

3) A contingency management scheme (CMS) of IEGS is devised to minimize the load curtailments and deviations to AGCR when system components fail. A detailed security-constrained optimal energy flow model of IEGS with distributed alternative gas injections is developed, where the variations of physical characteristics (e.g., specific gravity) due to the varying gas compositions are considered. The topological change of the gas network due to multiple pipeline failure modes is formulated, where the concept of the virtual gas bus is introduced to model the gas leak effect.

4) A fast analytical long-term reliability evaluation procedure is designed. The second-order-cone reformulation, forward-approximation-based linearization, and Taylor approximation-based methods are tailored to transfer the original two-stage mixed-integer nonlinear CMS optimization problem into a more tractable second-order-cone programming problem. An adaptive scenario reduction technique is proposed by identifying and eliminating the common states and marginal states in different time intervals, so that the computation efficiency can be improved.

2. Structure of IEGS With Alternative Gas Injections

The structure of the IEGS with alternative gas injections is illustrated in Fig. 1. In the IEGS, the electricity and gas systems are interconnected by GPPs and PTGs. GPPs consume gas mixtures from the gas network to produce electricity, while PTGs consume electricity to produce methane and hydrogen. Along with other types of gases, such as biogas and natural gas, they can be injected into gas pipelines, and further satisfy the gas demands at various locations.
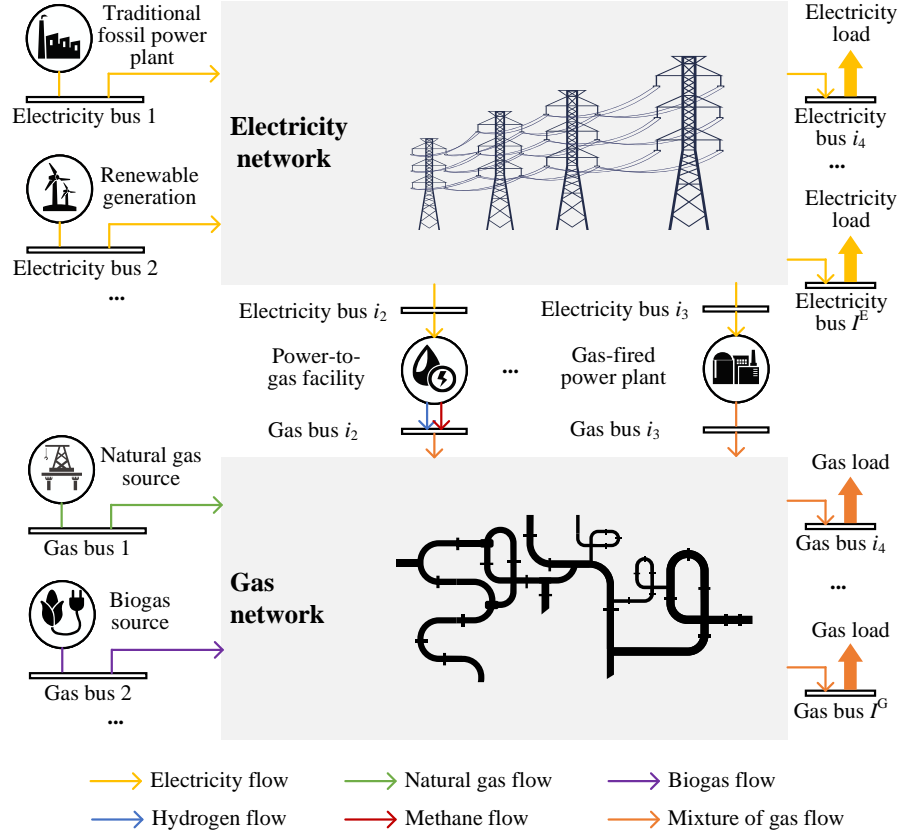
Figure 1: Structure of the IEGS with alternative gas injections.

3. Long-Term Reliability Indices for IEGS

Generally, the reliability of an engineering system can be defined as its capability to complete a certain task under the given condition [25]. In traditional IEGS with the constant gas composition, the reliability is usually defined by its capability of providing sufficient amounts of electricity and gas to consumers [26]. However, it is different for the IEGS with alternative gas injections due to the varying gas compositions. The gas appliances of consumers have specific requirements for gas compositions [27]. When some gas system components (e.g., gas sources, pipelines, etc.) fail, apart from the unserved loads, it is also possible that the gas compositions no longer meet the requirements of gas appliances. In another word, the interchangeability of the new gas mixture is not close enough to the original nature gas. Therefore, the reliability of IEGS in this paper is defined twofold, i.e., the capabilities to serve consumers with the gas in both adequate amounts and satisfactory interchangeability.

6

3.1. Reliability Indices for Gas Adequacy

Derived from the commonly used reliability indices in the electricity systems, i.e., expected demand not supplied (EDNS) and loss of load probability (LOLP), the reliability indices for the gas systems, i.e., the expected gas not supplied (EGNS) and loss of gas load probability (LOGP), are defined as:
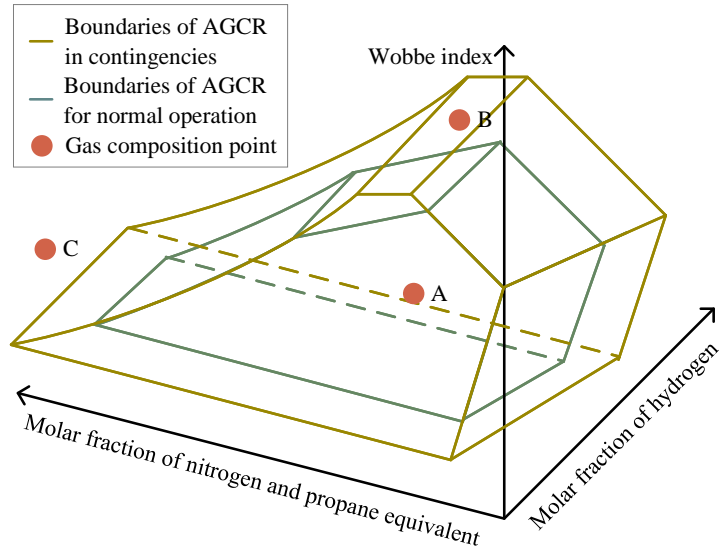
$$EGNS_{i,t} = \sum_{s \in \mathcal{S}} \text{Pr}_{s,t} \sum_{r \in \mathcal{R}} q_{i,r,s,t}^{ct} \tag{1}$$

$$LOGP_{i,t} = \sum_{s \in \mathcal{S}} \text{Pr}_{s,t} flag\left(\sum_{r \in \mathcal{R}} q_{i,r,s,t}^{ct} > 0\right) \tag{2}$$

where i is the index for bus; t is the index for the time interval in the long-term reliability evaluation. The time interval can be one year, one month, etc., depending on the requirement for the time resolution. $EGNS_{i,t}$ and $LOGP_{i,t}$ are the EGNS and LOGP at gas bus i in time interval t, respectively; s is the index for system state; $\mathcal{S}$ is the set of all possible system states; $\text{Pr}_{s,t}$ is the probability of system state s in time interval t. For each time interval $t \in \mathcal{T}$, where $\mathcal{T}$ is the set of time interval, $\sum_{s \in \mathcal{S}} Pr_{s,t} = 1$. r is the index for gas composition, and $\mathcal{R}$ is the set of gas composition; $q_{i,r,s,t}^{ct}$ is the gas load curtailment of gas component r at bus i in system state s in time interval t; $flag(\cdot)$ is a flag function, where $flag(\cdot) = 1$ indicates the expression $(\cdot)$ is true; $flag(\cdot) = 0$ indicates the expression $(\cdot)$ is false.

3.2. Reliability Indices for Gas Interchangeability

The measurement for gas interchangeability varies by country and region. Among many criteria, the Dutton diagram is one of the most typical methods that is widely adopted in the UK, Western Australia, etc [28]. The Dutton diagram outlines the AGCR, as presented in Fig.2. The upper half of Fig.2 is the 3-D Dutton diagram, and the lower half of Fig.2 is its projection on the "Molar fraction of nitrogen and propane equivalent"-"Wobbe index" plane. The 3-D Dutton diagram consists of three axes: the molar fraction of nitrogen and propane equivalent, the molar fraction of hydrogen, and the Wobbe index (WI). Three indices, i.e., WI, incomplete combustion factor (ICF), and soot index (SI), are employed to limit the gas composition in the Dutton diagram. They
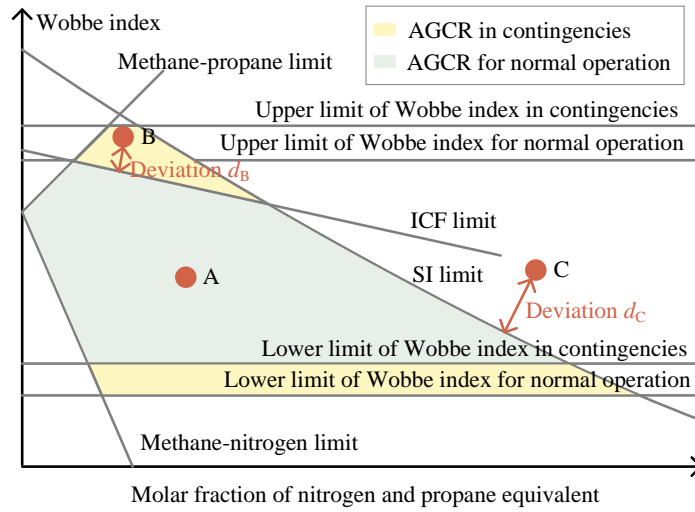
Figure 2: Dutton diagram and acceptable gas composition regions.

can be calculated as [29, 30] (the notation s and t are omitted):

$$WI_i = GCV_i SG_i^{-\frac{1}{2}} \tag{3}$$

$$ICF_i = (WI_i - 50.73 + 0.03x_i^{np})/1.56 - 0.01x_i^{hy} \tag{4}$$

$$SI_i = 0.896 tan^{-1}(0.0255x_i^{pr} - 0.0233x_i^{ni} - 0.0091x_i^{hy} + 0.617) \tag{5}$$

where WI_i, ICF_i, and SI_i are the WI, ICF, and SI at bus i, respectively; GCV_i and SG_i are the GCV and specific gravity of the gas at bus i, respectively; x_i^{np} is the total molar fraction of propane and nitrogen; x_i^{hy}, x_i^{pr}, and x_i^{ni} are the molar fractions of hydrogen, propane, and nitrogen, respectively.

In the normal operation, the boundaries for ICF, SI, WI, and molar fraction of hydrogen, as well as two physical boundary lines (i.e., methane-propane limit and methane-nitrogen limit) delineate the AGCR in (6) [31]. In the contingencies, relaxations of ICF, WI, and molar fraction of hydrogen are temporarily allowed. The AGCR in the normal operation, $\mathbb{F}^{NO}$, are defined as follows:

$$\mathbb{F}^{NO} = \left\{ \boldsymbol{x}_i \mid WI^{NO,min} \le WI_i \le WI^{NO,max}; ICF^{NO,min} \le ICF_i \le ICF^{NO,max}; \right.$$
$$\left. SI^{min} \le SI_i \le SI^{max}; 0 \le x_i^{hy} \le x^{hy,NO,max}; \boldsymbol{0} \le \boldsymbol{x}_i \le \boldsymbol{1}; \boldsymbol{1}^T \boldsymbol{x}_i = 1; \right\} \tag{6}$$

where $\boldsymbol{x}_i$ is the set of molar fractions of gas compositions at bus i; $ICF^{NO,max}$, $WI^{NO,max}$, $x^{hy,NO,max}$, $ICF^{NO,min}$, $WI^{NO,min}$, and $x^{hy,NO,min}$ are the upper and lower bounds for ICF, WI, and molar fraction of hydrogen in the normal operating state, respectively; SI^{max} and SI^{min} are the upper and lower bounds for SI, respectively. The AGCR in contingency states $\mathbb{F}^{CO}$ can be defined similarly.

The gas interchangeability depends on the gas composition (i.e., the coordinate of the gas composition in the Dutton diagram). As aforementioned, the AGCR in contingencies is wider than that in normal operations. Denote the extra AGCR in contingencies (the yellow area in the lower half of Fig. 2) as $\mathbb{F}^{EX}$ ($\mathbb{F}^{EX} = \mathbb{F}^{CO} - \mathbb{F}^{NO}$). For example, as shown in Fig. 2, the gas composition of point A $\boldsymbol{x}^A \in \mathbb{F}^{NO}$ is acceptable; for $\boldsymbol{x}^B \in \mathbb{F}^{EX}$,

9

it is acceptable in contingencies, while not acceptable in normal operations; $\boldsymbol{x}^C \notin \mathbb{F}^{CO}$ is an unacceptable gas composition. With this idea in mind, two reliability indices are defined, namely, expected gas interchangeability deviation (EGID) and gas interchangeability deviation probability (GIDP), as calculated in (7) and (8), respectively. GIDP measures the probability of gas composition that fall out of the AGCR. EGID measures the expected deviations of the gas composition to the AGCR.

$$EGID_{i,t} = \sum_{s \in \mathcal{S}^{NO}} \Pr_{s,t} d_{i,s,t}^{NO} + \sum_{s \in \mathcal{S}^{CO}} \Pr_{s,t} d_{i,s,t}^{CO} \tag{7}$$

$$GIDP_{i,t} = \sum_{s \in \mathcal{S}^{NO}} \Pr_{s,t} \left(flag(\boldsymbol{x}_{i,s,t} \notin \mathbb{F}^{NO}) \right) + \sum_{s \in \mathcal{S}^{CO}} \Pr_{s,t} \left(flag(\boldsymbol{x}_{i,s,t} \notin \mathbb{F}^{CO}) \right) \tag{8}$$

where $EGID_{i,t}$ and $GIDP_{i,t}$ are the EGID and GIDP at bus i at time interval t, respectively; $\mathcal{S}^{NO}$ and $\mathcal{S}^{CO}$ are the sets of normal operating state and contingency state, respectively; $d_{i,s,t}^{NO}$ and $d_{i,s,t}^{CO}$ are the deviations to the AGCR in normal operation and contingencies for bus i in state s at time interval t, respectively; $d_{i,s,t}^{NO}$ can be calculated by:

$$d_{i,s,t}^{NO} = \min_{\boldsymbol{x}_i^O \in \mathbb{F}^{NO}} \|\boldsymbol{x}_i - \boldsymbol{x}_i^O\| \tag{9}$$

where $\boldsymbol{x}_i^O$ is a gas composition point within the AGCR in normal operation or contingency at bus i; $d_{i,s,t}^{CO}$ can be calculated similarly.

4. Reliability Models of IEGS Components

4.1. Multi-State Reliability Model of Pipeline Considering Corrosion Effect

During the long-term operation, the pipeline gradually corrodes due to environmental issues and hydrogen injections. There are three pipeline failure modes caused by corrosion, namely, small leak, large leak, and rupture [32]. The limit state functions associated with the small leak, large leak, and rupture failure for the segment l in the pipeline that connects bus i and bus j (denoted as pipeline ij) are $f_{i,j,l}^{sl}$, $f_{i,j,l}^{ll}$, and $f_{i,j,l}^{rp}$,
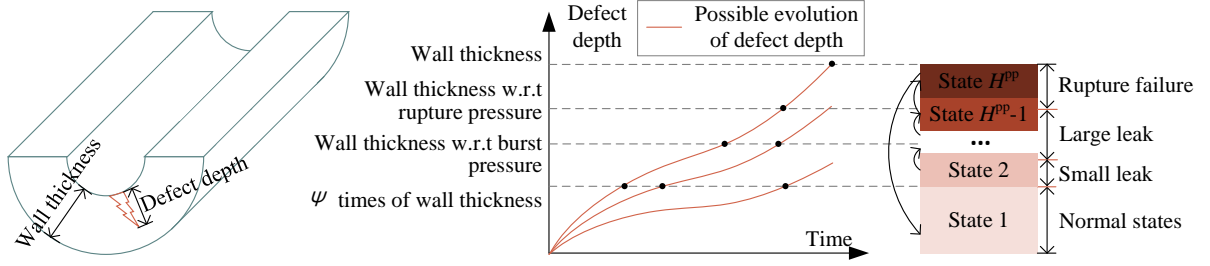
Figure 3: Multi-state reliability model of the pipeline considering corrosion.

respectively. They can be calculated by [33]:

$$f_{i,j,l}^{sl} = \psi wt_{i,j} - \delta_{i,j,l} \tag{10}$$

$$f_{i,j,l}^{ll} = \kappa p_{i,j,l}^{bs} - p_{i,j,l} \tag{11}$$

$$f_{i,j,l}^{rp} = \kappa p_{i,j,l}^{rp} - p_{i,j,l} \tag{12}$$

where $wt_{i,j}$ is the wall thickness of the pipeline ij; $\delta_{i,j,l}$ is the defect depth of segment l in pipeline ij; ψ is the coefficient for small leak failure, which indicates that the corrosion could lead to small leak if the defect depth exceeds ψ times of wall thickness; $p_{i,j,l}^{bs} = f_{bs}(\delta_{i,j,l})$ and $p_{i,j,l}^{rp} = f_{rp}(\delta_{i,j,l})$ are the burst pressure and rupture pressure, respectively. They are the functions of defect depth, which are elaborated in Appendix A; $p_{i,j,l}$ is the gas pressure of segment l in pipeline ij during the operation; κ is the hydrogen damage factor, which is also introduced in Appendix A [34]. The pipeline failure mode depends on the values of limited state functions. If $f_{i,j,l}^{sl} \leq 0$ and $f_{i,j,l}^{ll} > 0$, a small leak occurs; if $f_{i,j,l}^{sl} > 0$, $f_{i,j,l}^{ll} \leq 0$, and $f_{i,j,l}^{rp} > 0$, a large leak occurs; if $f_{i,j,l}^{sl} > 0$, $f_{i,j,l}^{ll} \leq 0$, and $f_{i,j,l}^{rp} \leq 0$, a rupture occurs; in other situations, the pipeline is at normal operation state [22].

The corrosion of the pipeline grows over time. The shape of the corrosion consists of two dimensions: defect length and defect depth. According to typical industry practice, the defect depth is more critical that influences the availability of the pipeline [35]. The growth of defect depth at each pipeline segment can be represented by an independent and homogeneous gamma process $f^{gm}(\cdot)$[36]:

$$f^{gm}(\delta_{i,j,l,t}|\alpha,\beta) = \left(\beta^{\alpha(t-t_0)}\delta_{i,j,l}^{\alpha(t-t_0)-1}e^{-\beta\delta_{i,j,l,t}}\right)/\Gamma\left(\alpha(t-t_0)\right), t \geq t_0 \tag{13}$$

where α and β are the shape parameters of the gamma process; $\Gamma(\cdot)$ is the gamma function.

The above gamma process is time-continuous. The defect depth in any time t can also take a continuous random value in $[0, wt]$. To reduce the computation burden, we develop a multi-state model to represent the gamma process for the pipeline by using the reliability network equivalent technique [37], as shown in Fig. 3. In this model, the continuous defect depth can be divided into H^{pp} non-overlapping intervals. At each time interval, the defect depth takes a random value from $\{\delta_{i,j,l}^1, ..., \delta_{i,j,l}^h, ..., \delta_{i,j,l}^{H^{pp}}\}$. To reduce the system states, the selection of the pipeline states should be efficient, which means the different system operating conditions can be reflected with minimum pipeline states. Taking the segment l in pipeline ij as an example, the defect depths of the first state (the normal operating state, $h = 1$) and the rest of the states ($h = 2, 3, ..., H^{pp}$) are divided by:

$$\delta_{i,j,l}^h = \begin{cases} \min\left\{f_{bs}^{-1}(p_{i,j,l}^{bs}), f_{rp}^{-1}(p_{i,j,l}^{rp}), \psi wt_{i,j}\right\}, & h = 1 \\ \left(wt_{i,j} - \delta_{i,j,l}^1\right) / \left(H^{pp} - 1\right), & h = 2, 3, ..., H^{pp} \end{cases} \tag{14}$$

The probability of the defect depth falling in state $h = 1$ at time interval t can be calculated by:

$$\Pr\left\{\delta_{i,j,l,t} = \delta_{i,j,l}^h\right\} = \int_{(t-1)\Delta t}^{t\Delta t} \int_0^{\delta_{i,j,l}^h} f^{gm}(\delta_{i,j,l,\tau}) \mathrm{d}\delta \mathrm{d}\tau, \ h = 1 \tag{15}$$

where Δt is the length of the time interval. The probability of other states can be calculated similarly.

4.2. Multi-State Reliability Models of Other Components

Without loss of generality, the reliabilities of other IEGS components, including renewable generators, traditional fossil-fueled power plants (which consume other fossils other than gas), GPPs, gas sources, PTGs, and electricity branches, are described by the multi-state Markov model. Here we use GPP as an example, other components can be modeled similarly.

The GPP is usually a complex engineering system that consists of many elements. The partial failure of the elements does not necessarily lead to the complete failure of the GPP. Therefore, the reliability of the GPP can be represented by a multi-state model. Generally, GPP k at bus i has H^{gpp} states. The electricity generating capacity in state h
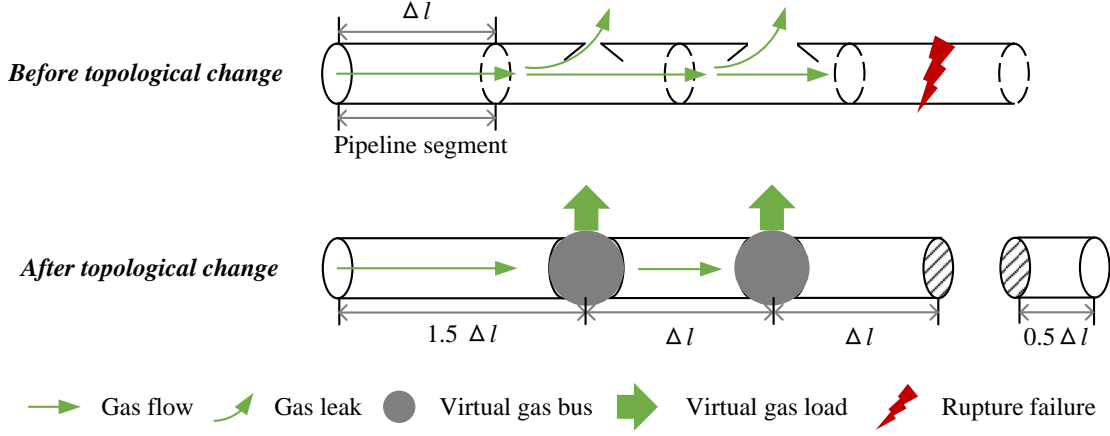
12

Figure 4: Topological change of the gas network with different pipeline failure modes.

is denoted as $g_{i,k}^{h,max}$. Due to random failures and repairs, the generating capacity of GPP $g_{i,k}^{gpp}$ takes random value from $\{g_{i,k}^{1,max}, ..., g_{i,k}^{h,max}, ..., g_{i,k}^{H^{GPP},max}\}$. The state probabilities can be calculated by solving the following state transition partial derivative equations:

$$\begin{cases} \dfrac{\mathrm{d}\mathrm{Pr}_h^{gpp}(t)}{\mathrm{d}t} = -\mathrm{Pr}_h^{gpp} \sum_{h'=1}^{H^{gpp},h'\neq h} \lambda_{h,h'} + \sum_{h'=1}^{H^{gpp},h'\neq h} \mathrm{Pr}_{h'}^{gpp}\lambda_{h',h}, \quad h = 1,2,...,H^{gpp} \\ \\ \mathrm{Pr}_1^{gpp}\mid_{t=t_0}= 1, \ \mathrm{Pr}_2^{gpp}\mid_{t=t_0}= ... = \mathrm{Pr}_{H^{gpp}}^{gpp}\mid_{t=t_0}= 0 \end{cases} \tag{16}$$

where Pr_h^{gpp} is the probability of the GPP in state h; $\lambda_{h,h'}$ is the state transition rate from state h to h'. The steady-state probability of state h equals to the solution of $\mathrm{Pr}_h^{gpp}(t)\mid_{t\to\infty}$.

5. Contingency Management Scheme of IEGS

The electricity and gas loads of consumers rely on the normal functioning of the IEGS components. Failures of components may transfer the IEGS from the normal operating state to the contingency state. The gas composition may change dramatically and even violate the AGCR. The supplies to the electricity and gas loads may also be interrupted. Therefore, a contingency management scheme (CMS) is developed to minimize the load curtailments and the deviations to the AGCR when the component fails.

5.1. Change of Gas Network Topology Considering Different Pipeline Failure Modes

The failures of pipelines can dramatically change the gas flow pattern in the gas network. In the gas leak failure mode, some gas in the pipeline will be released to the outside, which means the inlet gas of the pipeline does not equal the outlet gas, as

13

presented in Fig. 4. In the rupture failure, the adjacent gas buses will act immediately (such as closing the valves) to prevent secondary risk. Therefore, the topology of the gas network should be updated when different pipeline failure happens.

For a given pipeline ij, rupture failure has the top priority. Once the rupture failure happens at any segment of the pipeline, the pipeline is regarded to be isolated from the IEGS. The characteristic parameter of pipeline ij in the Weymouth function $C_{i,j}$ (introduced in (25) should be set to zero:

$$C_{i,j} = 0, \ ij \in \mathcal{P}^{rp} \tag{17}$$

where $\mathcal{P}^{rp}$ is the set of ruptured pipelines.

If there is no rupture failure in the pipeline ij, but gas leak failures (including small leak and large leak) happen in pipeline segment l ($l \in \mathcal{L}^{gl}$, where $\mathcal{L}^{gl} = \{l_1, ..., l_v, ..., l_V\}$ is the set of pipeline segments with gas leaks; v is the index of the gas leak; V is the number of gas leaks), the leakage can be regarded as a virtual gas load, and the leak position can be regarded as a virtual gas bus [38]. A set of virtual gas bus $\hat{\mathcal{I}}$ is introduced ($\hat{\mathcal{I}} = \{\hat{i}_1, ..., \hat{i}_V\}$) to model the new topology of the gas network with gas leaks. The lengths of the pipeline between the inlet bus i and the first virtual gas bus $\hat{i}_1$, the length of the pipeline between any two adjacent virtual gas buses $\hat{i}_v$ and $\hat{i}_{v+1}$, and the length of the pipeline between the last virtual gas bus $\hat{i}_V$ and outlet gas bus j are denoted as $L^N_{i,\hat{i}_1}$, $L^N_{\hat{i}_v,\hat{i}_{v+1}}$, and $L^N_{\hat{i}_V,j}$. They can be calculated by:

$$L^N_{i,\hat{i}_1} = (l_1 - 1)\Delta l + \Delta l/2 \tag{18}$$

$$L^N_{\hat{i}_v,\hat{i}_{v+1}} = (l_{v+1} - l_v)\Delta l \tag{19}$$

$$L^N_{\hat{i}_V,j} = (L - l_V)\Delta l + \Delta l/2 \tag{20}$$

where Δl is the length of a pipeline segment, $\Delta l = L^N/L$; L^N is the length of the pipeline, and L is the number of the segment in the pipeline.

The virtual gas load of the gas leak at the virtual gas bus $\hat{i}_v$ is denoted as $q^{gl}_{\hat{i}_v}$. It can

be calculated by [39]:

$$q_{\hat{i}_v}^{gl} = p_{\hat{i}_v} \frac{\pi \phi_{i,j,l_v}^2}{4} \left(\frac{M_{i,j}^W \gamma_{i,j}}{R^{gas} T^{gas}} \left(\frac{2}{\gamma_{i,j}+1} \right)^{\frac{\gamma_{i,j}+1}{\gamma_{i,j}-1}} \right)^{\frac{1}{2}} \qquad (21)$$

where ϕ_{i,j,l_v} is the defect length of the segment l_v in pipeline ij; $p_{\hat{i}_v}$ is the gas pressure at virtual gas bus $\hat{i}_v$; $M_{i,j}^W$ and $\gamma_{i,j}$ are the molecular weight and the heat capacity ratio of the gas mixture in pipeline ij, respectively [40]; R^{gas} is the gas constant; T^{gas} is the temperature of the gas.

5.2. Gas Network Model With Alternative Gas Injections and Pipeline Failures

With the varying gas composition, the GCVs of the gas mixtures may also vary at different locations. Thus, the volume of the gas load is subject to the GCV at the exact location:

$$q_i^{d,ng} GCV^{ng} = GCV_i \sum_{r \in \mathcal{R}} \left(q_{i,r}^d + q_{i,r}^{ct} \right) \qquad (22)$$

$$q_{i,r}^d / \sum_{r \in \mathcal{R}} q_{i,r}^d = x_{i,r} \qquad (23)$$

where $q_i^{d,ng}$ is gas demand at bus i measured by the volume of natural gas (without blending other types of gases); GCV^{ng} is the GCV of natural gas; $q_{i,r}^d$ is the gas demand of gas composition r at bus i; $x_{i,r}$ is the molar fraction of gas composition r at bus i.

The gas supplies from the gas sources also have various gas compositions, which can be represented by:

$$q_{i,k,r}^{gs} = x_{i,k,r}^{gs} \sum_{r \in \mathcal{R}} q_{i,k,r}^{gs} \qquad (24)$$

where $q_{i,k,r}^{gs}$ is the gas supply of gas composition r of gas source k at bus i; $x_{i,k,r}^{gs}$ is the molar fraction of gas composition r of the gas supply from gas source k at bus i.

In the gas transmission pipeline, the Weymouth equation can be used to describe the relations between the steady-state gas flow and gas pressures. For any two connected gas buses (including virtual gas bus), (25) and (26) are satisfied. The pipeline property parameter $C_{i,j}$ is calculated by (27). It should be noted that: 1) due to the varying gas composition, the specific gravity $SG_{i,j}$ and compressibility factor $Z_{i,j}$ of the gas mixture

15

also become variables; 2) due to the pipeline failure, the length of the pipeline depends on the new gas network topology according to Section 5.1.

$$q_{i,j}|q_{i,j}| = C_{i,j}^2(p_i^2 - p_j^2), \ i,j \in \mathcal{I}^G \cup \hat{\mathcal{I}} \tag{25}$$

$$q_{i,j} = \sum_{r \in \mathcal{R}} q_{i,j,r}, \ q_{i,j,r} \geq 0 \tag{26}$$

$$C_{i,j} = \frac{T^{stp}}{8p^{stp}} \left(\frac{\pi^2 D_{i,j}^5}{F_{i,j} SG_{i,j} L_{i,j}^N Z_{i,j} T^{gas}} \right)^{\frac{1}{2}} \tag{27}$$

$$|q_{i,j}| \leq q_{i,j}^{max} \tag{28}$$

$$p_i^{min} \leq p_i \leq p_i^{max}, \ i \in \mathcal{I}^G \cup \hat{\mathcal{I}} \tag{29}$$

where $q_{i,j}$ is the gas flow in the gas pipeline ij; p_i and p_j are the nodal gas pressures at bus i and bus j, respectively; $\mathcal{I}^G$ is the set of gas buses; $q_{i,j,r}$ is the gas flow of gas composition r in pipeline ij; T^{stp} and p^{stp} are the temperature and pressure at standard temperature and pressure condition, respectively; $D_{i,j}$, $F_{i,j}$, and $L_{i,j}^N$ are the diameter, friction factor, and length of the pipeline ij, respectively; $q_{i,j}^{max}$ is the transmission capacity of pipeline ij; p_i^{max} and p_i^{min} are the upper and lower bounds of the gas pressure at bus i, respectively.

The gases transported from upstream pipelines are mixed at the gas bus, and then the new gas mixture will be transported through downstream pipelines. During this process, the nodal gas conservation holds, but takes different forms at gas buses and virtual gas buses:

$$\sum_{k \in \mathcal{K}_i^{gs}} q_{i,k,r}^{gs} - q_{i,r}^d + \sum_{k \in \mathcal{K}_i^{ptg}} q_{i,k,r}^{ptg} - \sum_{k \in \mathcal{K}_i^{gpp}} q_{i,k,r}^{gpp} - \sum_{j \in \mathcal{J}_i} q_{i,j,r} - \sum_{j \in \hat{\mathcal{I}}_i} q_{i,j,r} = 0, \ i \in \mathcal{I}^G \tag{30}$$

$$q_{\hat{i}_{v-1}, \hat{i}_v, r} + q_{\hat{i}_v, r}^{gl} = q_{\hat{i}_v, \hat{i}_{v+1}, r}, \ \hat{i}_v \in \hat{\mathcal{I}} \tag{31}$$

where $\mathcal{K}_i^{gs}$, $\mathcal{K}_i^{ptg}$, and $\mathcal{K}_i^{gpp}$ are the sets of gas sources, PTGs, and GPPs at bus i, respectively; $\mathcal{J}_i$ is the set of bus connected to bus i; $q_{i,k,r}^{ptg}$ is the gas production of gas component r of PTG k at bus i; $q_{i,k,r}^{gpp}$ is the gas consumption of gas component r of GPP k at bus i.

The mixing process depends on the direction of the gas flow, which may change substantially from that in the normal operating state if severe failures happen. Therefore, we run a gas flow direction identification problem first (which is introduced in the Ap-

pendix B) to identify the gas flow direction in each pipeline. Denote $\omega_{i,j} = 1$ if the gas flows from bus i to j in pipeline ij. Otherwise, $\omega_{i,j} = -1$. Then, the gas composition at bus i can be calculated as [30]:

$$w_{i,r} = \sum_{j \in (\mathcal{J}_i \cup \hat{\mathcal{I}}_i)} \frac{1 - \omega_{i,j}}{2} q_{i,j,r} + \sum_{k \in \mathcal{K}_i^{gs}} q_{i,k,r}^{gs} + \sum_{k \in \mathcal{K}_i^{ptg}} q_{i,k,r}^{ptg} \tag{32}$$

$$x_{i,r} = w_{i,r} / \sum_{r \in \mathcal{R}} w_{i,r}, \ i \in \mathcal{I}^G \tag{33}$$

where $w_{i,r}$ is the nodal gas injection of gas component r at bus i.

The gas composition in the downstream pipeline should equal the gas composition at the upper stream bus:

$$q_{i,j,r} = q_{i,j} \left((1 + \omega_{i,j}) x_{i,r} + (1 - \omega_{i,j}) x_{j,r} \right) / 2 \tag{34}$$

Then, the specific gravity and compressibility factor of the gas mixtures in the pipeline ij can be updated as:

$$SG_i = \sum_{r \in \mathcal{R}} M_r^W x_{i,r} / M^{W,air} \tag{35}$$

$$SG_{i,j} = ((1 + \omega_{i,j}) SG_i + (1 - \omega_{i,j}) SG_j) / 2 \tag{36}$$

$$Z_{i,j} = f^z(\boldsymbol{x}_i^{(0)}, \boldsymbol{x}_j^{(0)}, p_i^{(0)}, p_j^{(0)}) \tag{37}$$

where M_r^W is the molecular weight of gas component r; $f^z(\cdot)$ is the function for calculating the compressibility factor, which can be found in [41].

5.3. Contingency Management Scheme of IEGS Considering Gas System Securities

If some IEGS components fail, the CMS will be performed to minimize the potential consequences of the contingency. The goal of the CMS is to minimize the IEGS operation and load curtailment costs, as well as the gas composition deviations, as shown in (38) and (39). The optimization variables $\boldsymbol{u}$ includes: 1) nodal gas pressure p_i; 2) gas production of gas source $q_{i,k}^{gs}$; 3) gas demand for each gas component $q_{i,r}^d$; 4) hydrogen and methane productions of PTG $q_{i,k}^{hy}$ and $q_{i,k}^{me}$; 5) electricity consumption of PTG $g_{i,k}^{ptg}$; 6) electricity generations of traditional fossil power plant $g_{i,k}^{tpp}$, GPP $g_{i,k}^{gpp}$, and renewable generators $g_{i,k}^{rng}$; 7) gas consumption of GPP $q_{i,k}^{gpp}$; 8) phase angle of the voltage θ_i; 9)

17

gas composition $x_{i,r}$; 10) gas flow for each gas component in the pipeline $q_{i,j,r}$.

$$C^O = \sum_{i \in \mathcal{I}} \left(\sum_{k \in \mathcal{K}_i^{tpp}} f_{i,k}^{cst}(g_{i,k}^{tpp}) + \rho_i^G \sum_{k \in \mathcal{K}_i^{gs}} q_{i,k}^{gs} - \mu^{ptg} \sum_{k \in \mathcal{K}_i^{ptg}} q_{i,k}^{ptg} + \mu^G \sum_{r \in \mathcal{R}} q_{i,r}^{ct} + \mu^E g_i^{ct} \right) \quad (38)$$

$$\min_{\boldsymbol{u}} \quad C^T = C^O + \sum_{i \in \mathcal{I}} \left(\mu^I (\chi \min_{\boldsymbol{x}_i^O \in \mathbb{F}^{NO}} \|\boldsymbol{x} - \boldsymbol{x}_i^O\| + (1 - \chi) \min_{\boldsymbol{x}_i^O \in \mathbb{F}^{CO}} \|\boldsymbol{x} - \boldsymbol{x}_i^O\|) \right) \quad (39)$$

where C^O is the operational cost, and C^T is the total cost; $\mathcal{I}$ is the set of buses; $\mathcal{K}_i^{tpp}$ is the set of traditional fossil power plants at bus i; $f_{i,k}^{cst}(\cdot)$ is the generating cost function of traditional fossil power plant k at bus i; ρ_i^G is the gas production cost of the gas source at bus i; μ^{ptg} is the subsidy of the green gas production for PTGs; μ^G and μ^E are the penalty factors for gas load and electricity load curtailments, respectively, which can be derived from the customer damage function [42]; μ^I is the penalty factor for gas interchangeability deviations; χ is the indicator for contingency state, where $\chi = flag(s \in \mathcal{S}^{NO})$. $\chi = 1$ indicates it is in the normal operation, while $\chi = 0$ indicates it is in the contingency state.

The optimization model subjects to (3)-(6), (17)-(36), and following constraints:

1) PTG constraints: the gas production process of the PTG, including the electrolysis and methanation, can be represented as:

$$g_{i,k}^{ptg} \eta_{i,k}^{el} = q_{i,k}^{me} GCV^{me} / \eta_{i,k}^{me} + q_{i,k}^{hy} GCV^{hy} \quad (40)$$

$$q_{i,k}^{ptg} = \sum_{r \in \mathcal{R}} q_{i,k,r}^{ptg} = q_{i,k}^{me} + q_{i,k}^{hy}, \quad q_{i,k}^{me}, q_{i,k}^{hy} \geq 0 \quad (41)$$

$$0 \leq g_{i,k}^{ptg} \leq g_{i,k}^{h,ptg,max} \quad (42)$$

where $g_{i,k}^{ptg}$ is the electricity consumption of PTG k at bus i; $\eta_{i,k}^{el}$ and $\eta_{i,k}^{me}$ are the efficiencies of electrolysis and methanation processes of PTG k at bus i, respectively; GCV^{me} and GCV^{hy} are the GCVs of methane and hydrogen, respectively; $g_{i,k}^{h,ptg,max}$ is the upper bound of the electricity consumption of PTG k at bus i in state h, which is determined by the reliability model of the PTG.

2) GPP constraints: GPP consumes the gas mixtures from the gas system to generate

electricity:

$$g_{i,k}^{gpp} = \eta_{i,k}^{gpp} \sum_{r \in \mathcal{R}} q_{i,k,r}^{gpp} GCV_r, \ q_{i,k,r}^{gpp} \geq 0 \tag{43}$$

$$q_{i,k,r}^{gpp} / \sum_{r \in \mathcal{R}} q_{i,k,r}^{gpp} = x_{i,r} \tag{44}$$

where $\eta_{i,k}^{gpp}$ is the efficiency of GPP k at bus i; GCV_r is the GCV of gas component r.

3) Electricity network constraints: the electricity network is modeled as:

$$\sum_{k \in \mathcal{K}_i^{tpp}} g_{i,k}^{tpp} + \sum_{k \in \mathcal{K}_i^{gpp}} g_{i,k}^{gpp} + \sum_{k \in \mathcal{K}_i^{rng}} g_{i,k}^{rng} - \sum_{k \in \mathcal{K}_i^{ptg}} g_{i,k}^{ptg} - g_i^d + g_i^{ct} - \sum_{j \in \mathcal{J}_i} g_{i,j} = 0 \tag{45}$$

$$g_{i,j} = (\theta_i - \theta_j)/X_{i,j} \tag{46}$$

$$|g_{i,j}| \leq g_{i,j}^{h,max} \tag{47}$$

$$g_{i,k}^{h,tpp,min} \leq g_{i,k}^{tpp} \leq g_{i,k}^{h,tpp,max} \tag{48}$$

$$g_{i,k}^{h,gpp,min} \leq g_{i,k}^{gpp} \leq g_{i,k}^{h,gpp,max} \tag{49}$$

$$g_{i,k}^{h,rng,min} \leq g_{i,k}^{rng} \leq g_{i,k}^{h,rng,max} \tag{50}$$

where g_i^d is the electricity demand at bus i; $g_{i,j}$ is the electricity flow on branch ij; $X_{i,j}$ is the reactance of branch ij; $g_{i,j}^{h,max}$ is the capacity of the electricity branch in state h; $g_{i,k}^{h,tpp,max}$, $g_{i,k}^{h,tpp,min}$, $g_{i,k}^{h,gpp,max}$, $g_{i,k}^{h,gpp,min}$, $g_{i,k}^{h,rng,max}$, and $g_{i,k}^{h,rng,min}$ are the upper and lower bounds of the traditional fossil power plant, GPP, and renewable generator in state h, respectively.

6. Long-Term Reliability Evaluation Procedures

6.1. Solution Methods for Contingency Management Scheme

In the long-term reliability evaluation, the CMS problem will be solved in each possible system state for many times under various stressful conditions. Therefore, the robustness and the computation time of solving each CMS problem will significantly influence the credibility and efficiency of the reliability evaluation. However, the CMS problem in its current form is a two-stage nonlinear programming problem, which can not be handled by commercial solvers properly and efficiently. Therefore, several reformulation techniques are developed to make the problem tractable.

1) Second-order cone relaxation and tightening of Weymouth equaitions:

Since the gas flow direction is pre-determined, (25) can be easily relaxed into the following second-order cone constraints:

$$p_i^2 - p_j^2 \geq q_{i,j}^2/C_{i,j}^2, \ \omega_{i,j} = 1 \tag{51}$$

$$p_j^2 - p_i^2 \geq q_{i,j}^2/C_{i,j}^2, \ \omega_{i,j} = -1 \tag{52}$$

To drive the relaxation exact, the term $\mu^{gf} \sum_{ij \in \mathcal{P}} w_{i,j} q_{i,j}$ are supplemented to the objective function (39), where $\mathcal{P}$ is the set of pipelines; μ^{gf} is the penalty factor for the gaps in Weymouth equations.

2) Relaxation and tightening for bilinear terms:

The bilinear terms exist in (23), (33), (34), and (44). Here we use a slack variable to approximate the new gas composition in the CMS around the gas composition in the normal operation. Taking (23) and (33) as examples, they can be relaxed into:

$$-\epsilon_{i,r}^d \leq x_{i,r}^{(0)} q_i^d - q_{i,r}^d \leq \epsilon_{i,r}^d, \ \epsilon_{i,r}^d \geq 0 \tag{53}$$

$$-\epsilon_{i,r}^{gb} \leq x_{i,r} \sum_{r \in \mathcal{R}} \omega_{i,r}^{(0)} + x_{i,r}^{(0)} \sum_{r \in \mathcal{R}} \omega_{i,r} - x_{i,r}^{(0)} \sum_{r \in \mathcal{R}} \omega_{i,r}^{(0)} - \omega_{i,r}^{(0)} \leq \epsilon_{i,r}^{gb}, \ \epsilon_{i,r}^{gb} \geq 0 \tag{54}$$

where $\epsilon_{i,r}^d$ and $\epsilon_{i,r}^{gb}$ are the slack variables; $x_{i,r}^{(0)}$ and $\omega_{i,r}^{(0)}$ are the gas composition and nodal gas injection of bus i for gas component r in the normal operation, respectively. Since the gas composition in the normal operation is in the AGCR, the constraints (53) can be also regarded as a measure to mitigate the deviations to the AGCR. The penalty terms $\mu^d \sum_{i \in \mathcal{I}} \sum_{r \in \mathcal{R}} \epsilon_{i,r}^d$ and $\mu^{gb} \sum_{i \in \mathcal{I}} \sum_{r \in \mathcal{R}} \epsilon_{i,r}^{gb}$ should be added to the objective function (39), where μ^d and μ^{gb} are the penalty factors.

3) Forward approximation of gas flow parameters:

We adopt a forward approximation-based method to estimate the values of the specific gravity and compressibility factor. First, we tentatively calculate the $SG_{i,j} = SG_{i,j}^{(0)}$, $Z_{i,j} = f^z(\boldsymbol{x}_i^{(0)}, \boldsymbol{x}_j^{(0)}, p_i^{(0)}, p_j^{(0)})$, where $SG_{i,j}^{(0)}$ and $p_i^{(0)}$ are the values of these variables in the normal operating state. Solve the CMS problem and obtain the new values as $SG^{(1)}$, $\boldsymbol{x}_i^{(1)}$, and $p_i^{(1)}$. Then, the value of $SG_{i,j}$ can be approximated by:

$$SG_{i,j} = \frac{1}{2} \left(SG_{i,j}^{(0)} + SG_{i,j}^{(1)} \right) \tag{55}$$

The value of $Z_{i,j}$ can be approximated similarly. Use these values to calculate the $C_{i,j}$ in (25), and solve the new CMS problem.

4) Taylor approximation of gas security constraints: Use Taylor expansion to approximate the WI in (3), and then substitute it into (6). Then, the security constraint of WI becomes:

$$WI_i^{min}\left((SG_i^{(0)})^{\frac{1}{2}} + SG_i(SG_i^{(0)})^{-\frac{1}{2}}\right) \leq 2GCV_i \leq WI_i^{max}\left((SG_i^{(0)})^{\frac{1}{2}} + SG_i(SG_i^{(0)})^{-\frac{1}{2}}\right) \tag{56}$$

The nonlinearity in (4) can be handled similarly.

5) Reformulation of objective function:

Add the penalty factors to the objective function (39), and convert it into a one-stage formulation:

$$\min_{\substack{u, \epsilon^d, \epsilon^{gb} \\ x_i^O \in \mathbb{F}'}} \quad C^T = C^O + \sum_{i \in \mathcal{I}} \mu^I \|x - x_i^O\| + \mu^{gf} \sum_{ij \in \mathcal{P}} w_{i,j}q_{i,j} + \sum_{i \in \mathcal{I}}\sum_{r \in \mathcal{R}}(\mu^d \epsilon_{i,r}^d + \mu^{gb} \epsilon_{i,r}^{gb}) \tag{57}$$

where $\mathbb{F}' = \mathbb{F}^{NO}$ when $\chi = 1$, and $\mathbb{F}' = \mathbb{F}^{CO}$ when $\chi = 0$.

6.2. Analytical Long-Term Reliability Evaluation Procedures With System State Reduction Techniques

The original long-term reliability evaluation of the IEGS with alternative gas can be divided into two stages. The first stage determines the evolution of pipeline corrosion. In each time interval t, the second stage is implemented to enumerate the state space with other component failures. Besides the reliability network equivalent technique that has been adopted in the reliability modeling of pipelines, here we further adopt two system state reduction techniques based on common states and marginal states:

1) Common state is defined as the system state which appears at more than one time interval. Due to the evolution of the pipeline states, the system states in each time interval change, but some of the states are common. By identifying these common states, over-calculation can be avoided.

2) Marginal state is defined as the system state where the transmission systems (electricity branches and gas pipelines) are intact, while other components (generators, gas sources, etc.) partially fail. It is assumed that the system in this paper is coherent

[43]. We identify some of the marginal states that have neglectable impacts on the final reliability evaluation results using the following criterion:

$$\max\left\{\Pr_{s,t}\sum_{i\in\mathcal{I}}\left(-g_i^d+\sum_{k\in\mathcal{K}^{gpp}}g_{i,k,s}^{gpp,max}+\sum_{k\in\mathcal{K}^{tpp}}g_{i,k,s}^{tpp,max}\right),\right.$$

$$\left.\Pr_{s,t}\sum_{i\in\mathcal{I}}\left(-q_i^{d,ng}GCV^{ng}+\sum_{k\in\mathcal{K}^{gs}}q_{i,k,s}^{gs,max}x_{i,k,r}^{gs}GCV_r+\sum_{k\in\mathcal{K}^{ptg}}g_{i,k,s}^{ptg,max}\eta_{i,k}^{el}\right)\right\}\le\zeta \quad (58)$$

where ζ is the threshold for neglectable marginal states.

The specific reliability evaluation procedures with the above system state reduction techniques are as follows:

Step 1: input the system data. Set the length of time interval Δt and the length of the total studied time intervals T. Set the parameters α and β for the Gamma process. Set the numbers of segments for pipelines. Set the defect depths in different pipeline states $\{\delta_{i,j,l}^1,...,\delta_{i,j,l}^h,...,\delta_{i,j,l}^{H^{pp}}\}$.

Step 2: for $t\in\mathcal{T}$, $ij\in\mathcal{P}$, and $h=\{1,...,h,...,H^{pp}\}$, calculate the probability of the pipeline segment being in each pipeline states according to Section 4.1. Calculate the defect depth, burst pressure, and rupture pressure in each state.

Step 3: calculate the state probabilities of IEGS components according to Section 4.2. Merge the state probabilities of pipelines and other components into the system state probability $\Pr_{s,t}$. Eliminate the common states and marginal states as described in the former contents in this section.

Step 4: for each system state, set the capacities of PTGs, electricity branches, traditional fossil power plants, GPPs, and renewable generators according to the states of components.

Step 5: solve the direction identification problem according to Appendix B. Obtain the gas flow direction $\omega_{i,j}$.

Step 6: solve the CMS problem with the prespecified gas flow direction and reformulation techniques according to Section 6.1. Obtain the gas pressures in pipelines.

Step 7: calculate the limit state functions in (10)-(12). Determine the failure modes for pipeline segments. If any pipeline failure occurs, go to **Step 8**. Otherwise, go to **Step 9**.
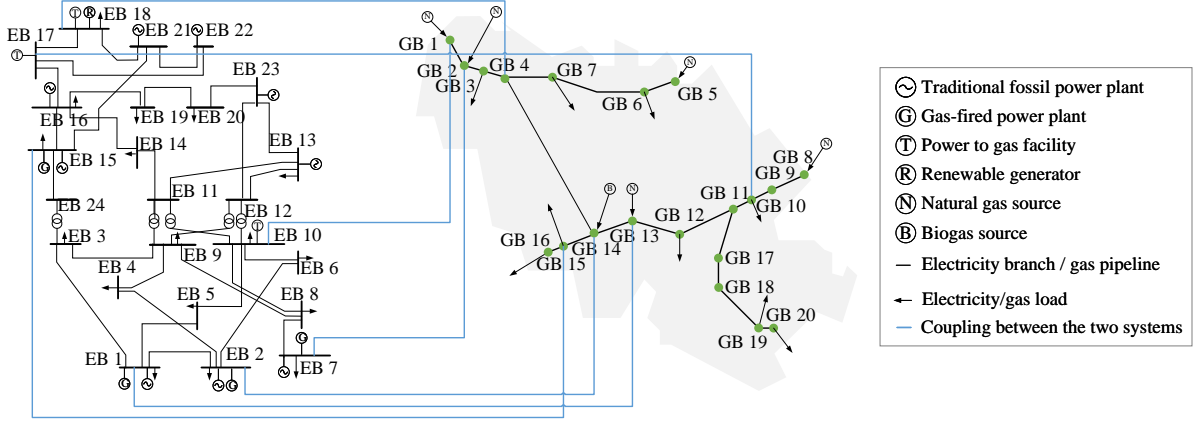
Figure 5: IEGS test system with alternative gas injections.

Step 8: update the topology and parameters of the gas network according to Section 5.1, and repeat the CMS in **Step 7**, until no additional topology update is required.

Step 9: obtain the results of the CMS. Obtain the electricity and gas load curtailments $g_{i,s,t}^{ct}$ and $q_{i,s,t}^{ct}$, and the deviations from AGCR $d_{i,s,t}^{NO}$ or $d_{i,s,t}^{CO}$.

Step 10: for each time interval t, summarize all the system states and calculate the reliability indices according to Section 3. The long-term reliability indices can be finally obtained.

7. Case Studies

An IEGS test case, composed of IEEE 24 bus Reliability Test System [44] and Belgium gas system [45], is used to validate the proposed long-term reliability evaluation technique. The two energy systems are topologically connected as Fig. 5. Several modifications are made: 1) the generators #1, #2, #5, #6, #9-#11, #16-#20 are replaced with GPPs; 2) PTGs of 3 Mm^3/day are installed at electricity bus #10, #17, and #18, respectively; 3) the gas compositions of the natural gas sources and biogas sources are set according to [15] and [8], respectively; 4) the 400 MW generators at electricity bus #18 and #21 are replaced by wind farms of the same capacity. The pipelines are made of X52 steel, and the wall thicknesses are determined according to [46]. The parameters of the Gamma process are set as $\alpha = 4$ year^{-1} and $\beta = 20$ mm^{-1} [22]. The time interval for reliability evaluation is one year. The total study period is 20 years. The complete data of the test case can be found in [47]. The simulation is performed on a desktop with Intel(R) Core(TM) i7-10700 CPU @2.9 GHz and 16 GB RAM.

Table 1: Representative system states

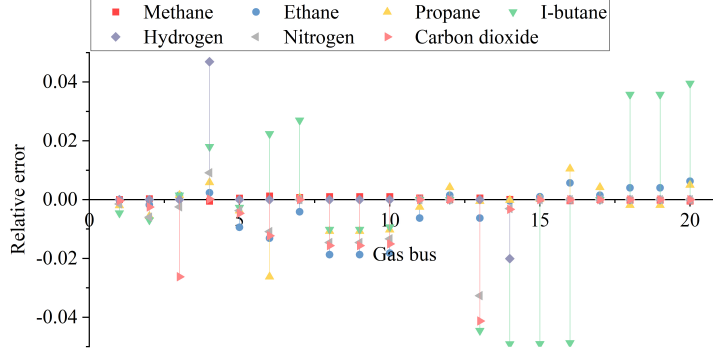| No.	Description of the system state
S1	Normal operating state
S2	Deration of gas source #1 at gas bus #1 by 2.32 Mm^3/day
S3	Deration of gas source #1 at gas bus #1 by 6.96 Mm^3/day
S4	Large leak of pipeline #7 between gas bus #4 and #14
S5	Rupture failure of pipeline #7 between gas bus #4 and #14
S6	Failure of 400 MW wind generator #23 at electricity bus #18

Figure 6: Relative errors of nodal gas compositions.

7.1. Case 1: Validation of Proposed CMS in the Representative System States

In case 1, as shown in Table 1, six representative system states are selected to demonstrate the effectiveness of the proposed CMS, as well as the impacts of component failures on the system conditions.

First, to validate the proposed reformulation and solution techniques, the numerical results of S1 using different solution methods are compared. We denote the solution method proposed in this paper as Method A, where the problem is solved by the Gurobi solver. Method B retains the nonlinear terms and is solved by the IPOPT solver. The relative errors of the two methods are presented in Fig.6. As we can see, most of the relative errors can be controlled within 1 %. The relative error of objective function values in these two methods is also controlled within 0.079%. Besides, the computation time of method A is 0.2110 s, which is 99.27 % faster than 33.49 s in method B.

To show the impacts of various failures on the IEGS, nodal gas compositions, gas productions of PTGs, gas load curtailments, deviations to AGCRs, and the security indices in the six system states are presented in Fig. 7, Fig. 8, and Fig. 9, respectively.

Observed from S1, S2, and S3, we find that the failures of gas sources not only lead to gas load curtailments, but also lead to the variation of gas composition, which may further endanger gas security. From S1 to S2, due to the partial failure of gas source #1, the gas productions of PTGs increase to cover the gas shortage, as shown in Fig. 8. (a), especially for PTG #1 at gas bus #1 and PTG #3 at gas bus #4. Thus, the hydrogen
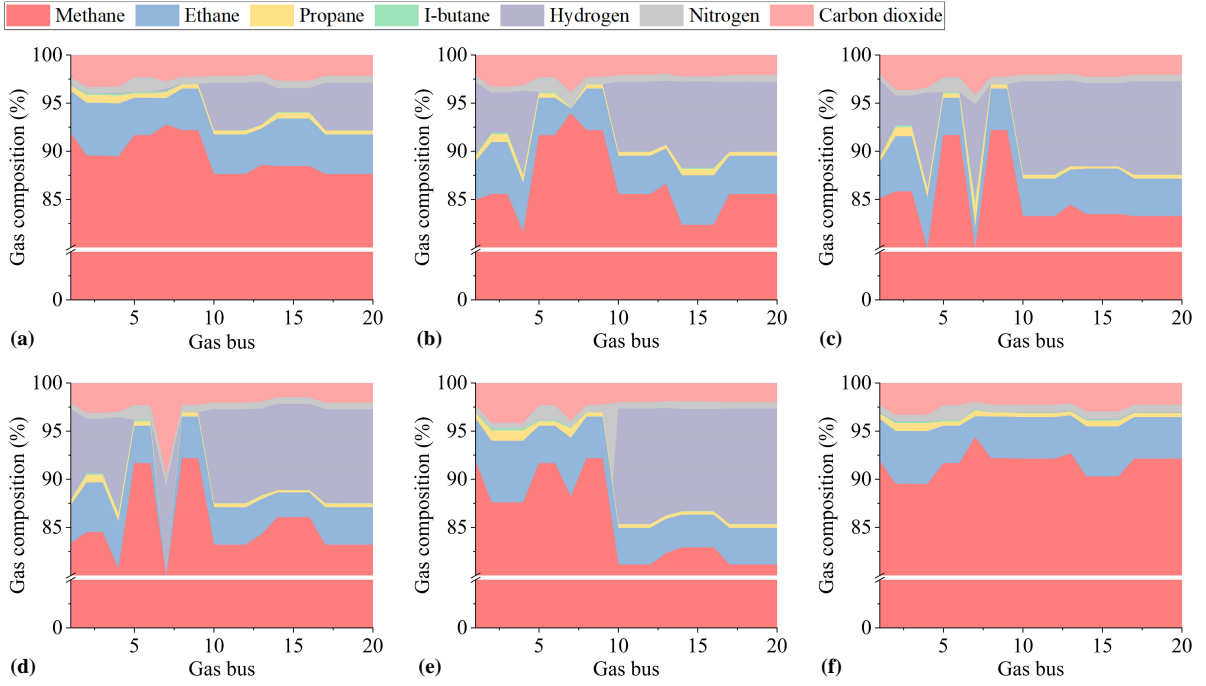
Figure 7: Gas compositions in different system states: (a) S1; (b) S2; (c) S3; (d) S4; (e) S5; (f) S6.
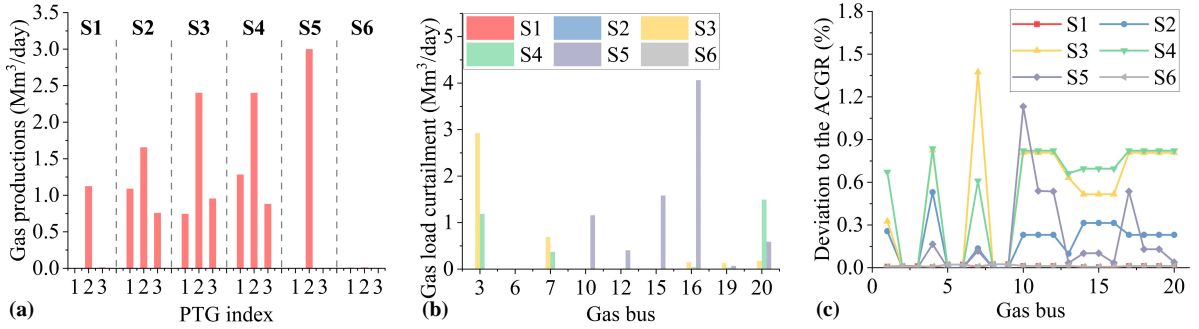

Figure 8: (a) Gas productions of PTGs; (b) gas load curtailments; (c) deviations to AGCRs.
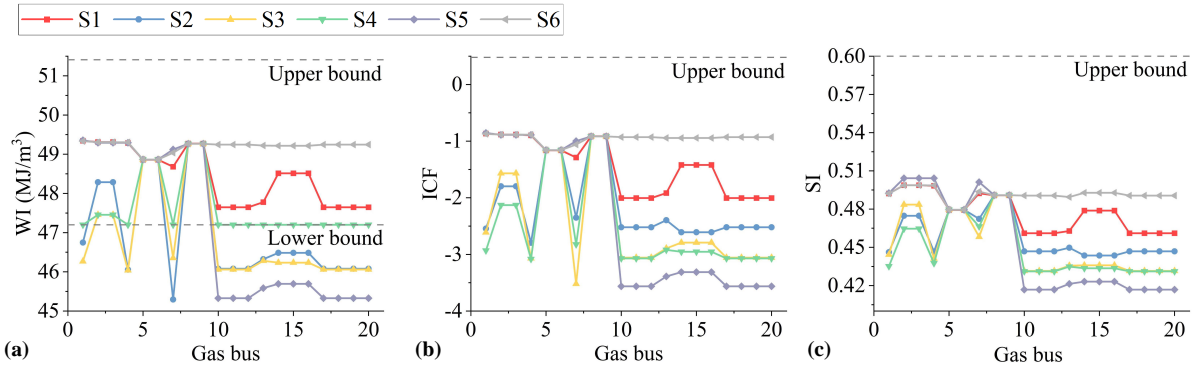

Figure 9: Security indices in different system states: (a) WI; (b) ICF; (c) SI.

proportions at gas buses #1-4 increase significantly, as shown in Fig. 7. (a). Besides, owing to the increase in the gas production of PTG #2 at gas bus #10, the hydrogen proportions at gas buses #10-20 also increase. Because the failure of gas source #1 is not very severe in S2, the gas shortage is covered by PTGs, and the gas load is not curtailed. However, due to the penetration of hydrogen, the gas composition deviated slightly from the AGCR. The ICF and SI are still within the secure limit, while the WI becomes lower than S1 and even violates the lower bound slightly, as shown in Fig. 9. As the failure of gas source #1 becomes more severe in S3, the gas productions of PTGs further increase, especially for PTG #2. Thus, the hydrogen proportions at gas buses #10-12 and #18-20 further increase. Nonetheless, the gas loads at gas buses #3, #16, #19, and #20 are still curtailed for 4.07 Mm^3/day. The deviations to AGCR are higher than S2, and the WI violates the lower bound more severely.

Observed from S1, S4, and S5, we find that different pipeline failure modes impact the IESG differently. For example, in S4, the large gas leak is equivalent to a 5.54 Mm^3/day virtual gas load between gas buses #4 and #14. Though the PTG gas production has increased to cover part of it, the gas loads at gas buses #3, #7, and #20 are still curtailed. The gas compositions and the WIs at many gas buses deviate from the AGCR. While in S5, though there are still large gas load curtailments, it is different spatially compared with S4. The gas load curtailment is mainly located at gas buses #10-20 in S5. The deviations to AGCR at gas bus #1 to #9 are relatively small, while it is larger at gas buses #10-20. This is because the rupture of gas pipeline #7 isolates the Belgium gas network into two parts, namely, the north part and the south part. In the north part, the gas supply is sufficient. The PTGs #1 and #3, which connect the north part, do not need to produce alternative gas. On the contrary, the gas supply in the south part is insufficient. The PTG #2, which connects the south part, reaches its maximum gas production capacity. Due to large amounts of hydrogen injections, the gas load curtailment is mitigated, but the gas interchangeabilities are sacrificed.

Comparing S1 and S6, we can also notice that the failure of renewable generations can also impact the gas compositions, for the PTGs mostly rely on them to produce gases. Therefore, the hydrogen productions of PTGs and the nodal hydrogen proportion are near zero in S6, and security indices are within the acceptable range.

Table 2: Scenario descriptions in case 2

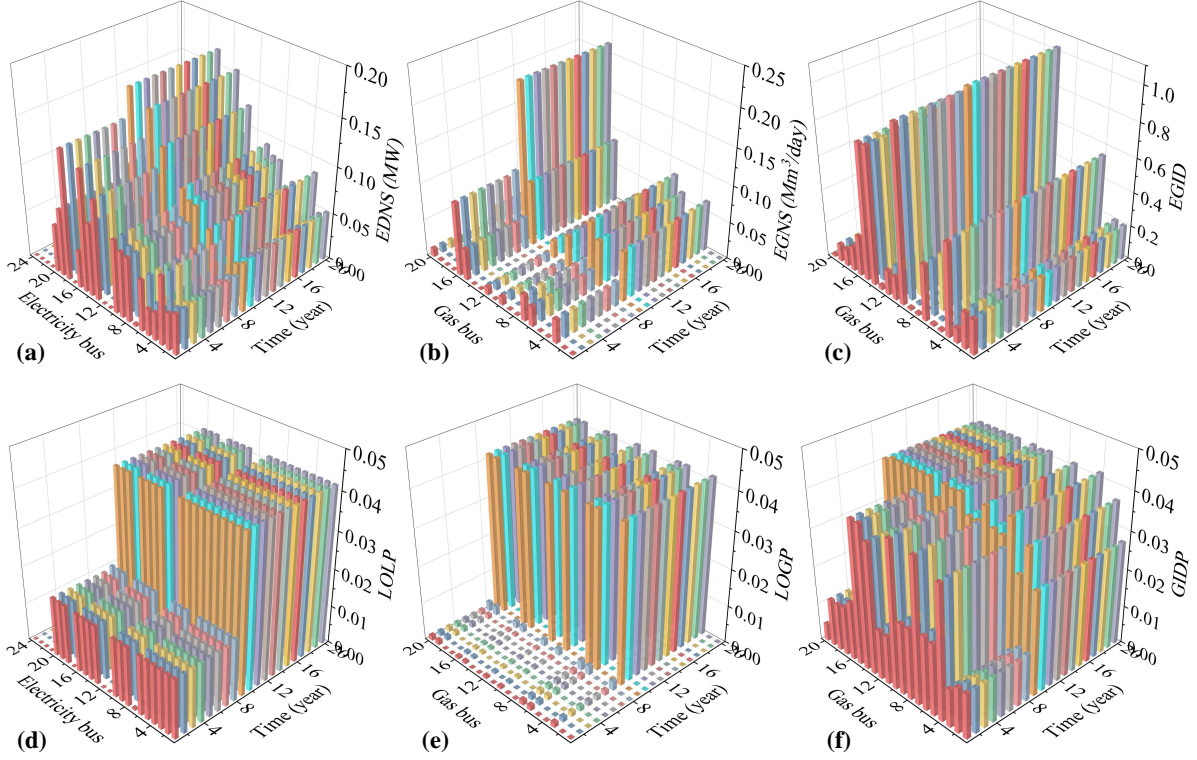| No.	Description of the scenario
S1	Base scenario
S2	The gas production capacities of PTGs increase to 6 Mm^3/day
S3	PTGs are reallocated at gas buses #16, #19, and #20, respectively
S4	The capacity of wind generator #23 is reduced to 200 MW, and another 200 MW wind generator is installed at electricity bus #1
S5	PTG is not installed
S6	Hydrogen embrittlement is not considered
S7	Corrosion of pipeline is not considered
S8	PTG is not installed, and hydrogen embrittlement is not considered

Figure 10: Long-term reliability indices in scenario S1: (a) EDNS; (b) EGNS; (c) EGID; (d) LOLP; (e) LOGP; (f) GIDP.

7.2. Case 2: Long-Term Reliability Indices of IEGS

In this case, we evaluate the long-term reliability indices of the IEGS, and compare the impacts of different factors on the IEGS reliability. The analytical method in this paper creates 970,200 system states in total. By using the scenario reduction technique, the effective system states are reduced to 26334 by 97.29%. With the reformulation techniques, the computation time is 9623 s, which is very efficient considering the study period of twenty years.

The long-term reliability indices of the IEGS are presented in Fig. 10. From the time dimension, we can see that the reliability indices grow over time, which means the reliability of IEGS is inferior due to the growth of pipeline corrosion. For example, in

pipeline #17, the probability of the perfect functioning state reduces to less than 10^{-3} after $t = 14$, if the repair is not considered. The total EDNS and EGNS of the system in $t = 20$ is 1.33 MW and 0.61 Mm^3/day, respectively, which increase by 20.91% and 125.37% than those in $t = 1$. We can also find a sudden increase in all the reliability indices between $t = 7$ and $t = 9$, especially for EGNS and LOGP. This is because the burst or rupture pressures for most pipelines are reduced to values that are very close to the normal operating pressure in $t = 7$. This could give us insights into the timing of pipeline inspections. For example, in our IEGS, the time period around $t = 7$ is a good time window to inspect and maintain the pipeline condition. Otherwise, the reliability of the IEGS may become much inferior shortly after $t = 7$.

We can also observe from the spatial dimension that the reliability indices vary in different buses. For example, gas bus #16 has the highest EGNS value among all the gas buses, accounting for about 34.11% of all the system EGNS. This is because gas bus #16 is at the end of a pipeline route, which is more prone to suffer load curtailment. It indicates that gas bus #16 is suggested to take measures to improve reliability, such as installing PTGs or distributed gas storage. Moreover, gas bus #10 has the highest EGID, which means it is more likely to suffer from unsatisfactory gas compositions. This is because gas bus # 10 is connected with electricity bus #17, where a 400 MW renewable generation and a 3 Mm^3/day PTG are installed. Under contingency states, it is more likely to inject alternative gas into gas bus # 10 to cover the gas shortage in the gas system. Therefore, the gas interchangeability may be sacrificed at gas bus #10. It indicates that gas bus #10 should pay more attention to gas security, and amendments could be made, such as injecting nitrogen or liquid petroleum gas.

To further analyze the impacts of different factors on the IEGS reliability, six additional scenarios are set and compared with the base scenario, as shown in Table 2. The long-term reliability indices are compared in Fig. 11.

Comparing S1, S2, and S5, we can see that the larger PTG capacity is beneficial for improving the overall reliability of IEGS. More specifically, as the PTG capacity increases, the EDNS is higher, while the EGNS is lower. The EGIDs in S1 and S2 are almost the same, while they are larger than the EGID in S5. This is because, with larger PTG capacities, the IEGS may use more electricity to produce hydrogen to cover the gas shortage when system components fail. Also due to the possible injection of hydrogen,
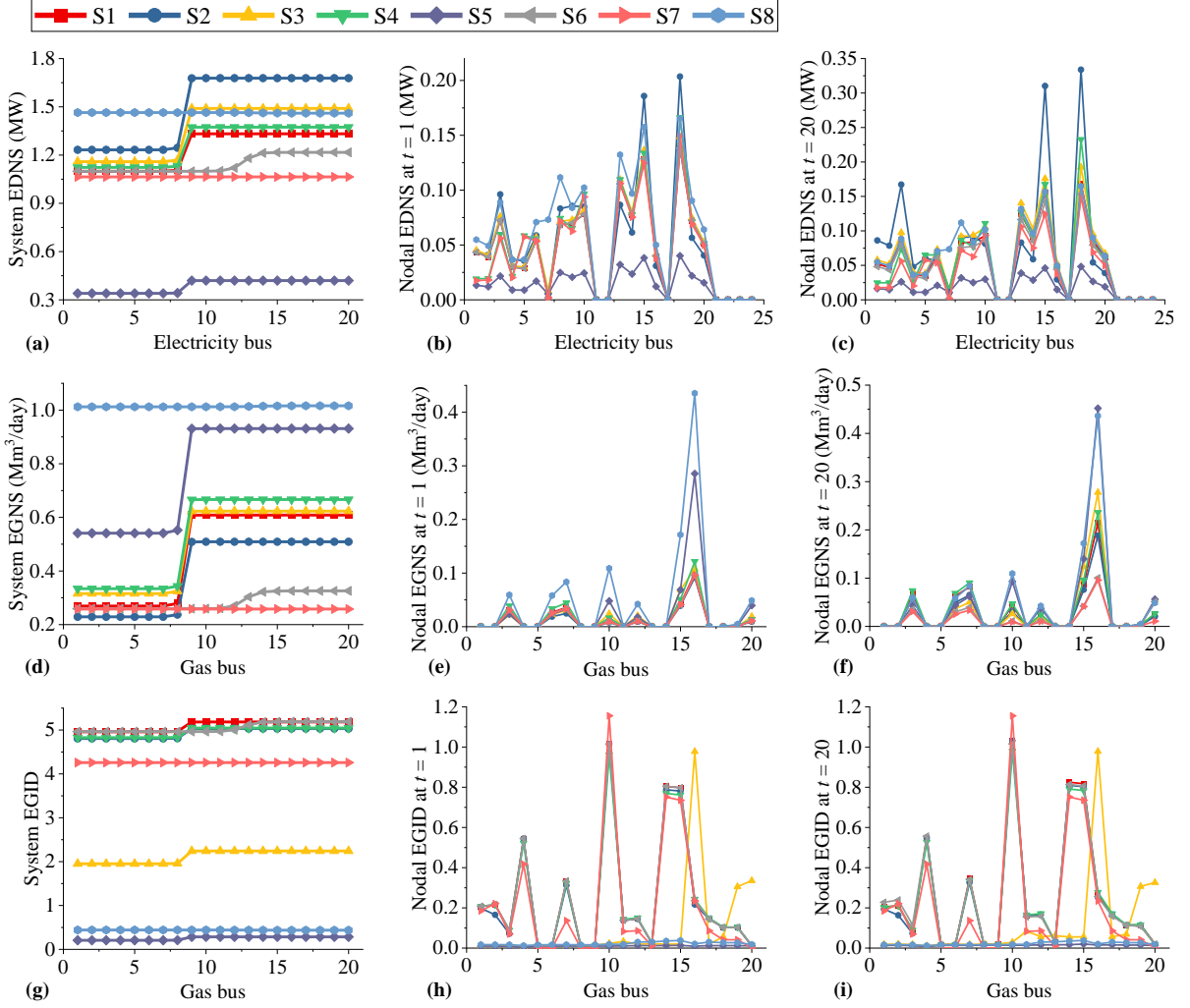
Figure 11: Comparisons of long-term reliability indices in different scenarios: (a) system EDNS; (b) nodal EDNS at $t = 1$; (c) nodal EDNS at $t = 20$; (d) system EGNS; (e) nodal EGNS at $t = 1$; (f) nodal EGNS at $t = 20$; (g) system EGID; (h) nodal EGID at $t = 1$; (i) nodal EGID at $t = 20$.

the gas compositions are more likely to violate the AGCR in S1 and S2 than in S5. From the time dimension, the reliabilities of all three scenarios become inferior with the growth of corrosion. Moreover, the impacts of corrosion vary in different systems, different buses, and different scenarios. The impact is more significant in the electricity system, such as electricity buses #15, #18 in S2, while less significant in the gas system, such as gas bus #15 in S5. This is because the electricity bus #15 has a GPP, which relies on the gas supply from the gas system. The larger PTG capacity requires a larger pipeline transmission capacity. Therefore, the corrosions of pipelines affect the electricity bus #15 more in S2. In contrast, in S5, the less PTG capacity has less requirement on the pipeline transmission capacity. Therefore, the corrosions of pipelines influence the EGNS of gas bus #15 less in S5.

Comparing S1, S3, and S4, we can also find that the relative location of PTGs and renewable generations also affects the IEGS reliability. In S3, all three PTGs are installed in the south part of the Belgium gas system. Both the EDNS and EGNS in the electricity and gas systems become inferior. The system EGID reduces because the PTGs have less opportunity to produce hydrogen. However, in the south part of the gas system, such as gas buses #10-20, the nodal EGID increases dramatically. This is because these gas buses are connected more closely to PTGs. In S4, the locations of renewable generators are more distant from the PTGs. Similar to S3, both the EDNS and EGNS in the electricity and gas systems become inferior compared with S1.

Comparing S1 and S6, we validate that the alternative gas injections do jeopardize the long-term reliability of IEGS. From Fig. 11.(a) and Fig. 11.(b), we can observe that in S6, the EDNS and EGNS are lower than in S1 by 7.58% and 39.73%, respectively. From the time dimension, the increases in EDNS and EGNS are deferred for about 3-4 years in S6. This is because, without hydrogen injection, the corrosion of the pipeline will be slower. This also indicates that it is necessary to consider the impact of hydrogen in the reliability evaluation of IEGS with alternative gases. Further comparing the reliability of S1, S6, and S8, we can find that though the injection of hydrogen can damage the reliability, it is still better than never injecting hydrogen at all. The EDNS and EGNS in S1 are 15.31% and 53.31% lower than in S8, respectively. If we can best mitigate or manage the corrosion of the pipeline (for example, conduct the in-line inspection more frequently and repair the corrosion more timely in the correct time window, e.g.,

$t = 8 - 9$ in the studied IEGS), the negative impacts of alternative gas on reliabilities can be minimized, as indicated by the reliability indices of S7.

8. Conclusions

This paper proposes a long-term reliability evaluation method for integrated electricity and gas systems considering the impacts of alternative gas injections. The numerical studies validate the effectiveness of the proposed method. The computation efficiency of the proposed solution method for the contingency management scheme is 99.27% higher than the traditional nonlinear solvers. The computation efficiency of the proposed long-term reliability evaluation method is 97.29% than the traditional enumeration-based method. Through comparative studies, we find that the relative locations and capacities of power-to-gas facilities and renewable generations can significantly impact the reliability of IEGS. We also conclude that the benefits of alternative gas injection outweigh the negative impacts. The alternative gas injections could jeopardize the reliability of the studied IEGS by 39.73%. However, with more frequent inspection and maintenance at the right time window ($t = 8 - 9$ year in our case), the reliability can be improved by up to 53.31%.

As alternative gas becomes more important in the decarbonization of energy systems, the reliability issues that come with it deserve our attention. With the help of the evaluation method and quantitative results in this paper, we are enabled to balance the losses and gains during the decarbonization of energy systems more accurately in the future.

Appendix A. Calculation of Burst Pressure and Rupture Pressure

The burst pressure of the pipeline is related to the corrosion condition, which can be calculated by:

$$p_{i,j,l}^{bs} = \xi \frac{2\sigma^{ut} wt_{i,j}}{D_{i,j}} \left(1 - \frac{\delta_{i,j,l}}{wt_{i,j}} \left(1 - \exp \left(\frac{-0.157\phi_{i,j,l}}{\sqrt{D_{i,j}(wt_{i,j} - \delta_{i,j,l})/2}} \right) \right) \right) \tag{A.1}$$

where $p_{i,j,l}^{bs}$ is the burst pressure of segment l of pipeline ij; ξ is the model error associated with the burst capacity model [48]; σ^{ut} is the ultimate tensile strength of the pipe steel.

The rupture pressure $p_{i,j,l}^{rp}$ can be calculated by:

$$p_{i,j,l}^{rp} = \left(1.8\sigma^{ut}wt_{i,j}\right) / \left(M^{fl}D_{i,j}\right) \tag{A.2}$$

where M^{fl} is the Folias factor[22].

The hydrogen damage factor is obtained through the regression analysis in [34]:

$$\kappa = 1.18736 - 0.08311T^{ch} + 0.01541(T^{ch})^2 - 0.0008927(T^{ch})^3 \tag{A.3}$$

where T^{ch} is the hydrogen charging time.

Appendix B. Gas Flow Direction Identification Problem

The gas flow direction identification problem is basically a steady-state optimal energy flow problem in IEGS. In this problem, because the varying gas composition does not cause a large gap in the operational condition of IEGS , the results of gas flow direction can be regarded as the same as the IEGS with varying gas composition. Therefore, the steady-state optimal energy flow problem is formulated as:

$$\min_{\boldsymbol{u}'} \quad C^O + \mu^{gf}\sum_{ij\in\mathcal{P}}\Phi_{i,j} \tag{B.1}$$

subject to (25), (27 - 29), (42), (45) - (50), and following constraints:

$$0 \leq g_{i,j}^{ct} \leq g_{i,j}^{ct,max} \tag{B.2}$$

$$0 \leq q_{i,j}^{ct} \leq q_{i,j}^{ct,max} \tag{B.3}$$

$$\sum_{k \in \mathcal{K}_i^{gs}} q_{i,k}^{gs} - q_i^{d,ng} + \sum_{k \in \mathcal{K}_i^{ptg}} q_{i,k}^{ptg} - \sum_{k \in \mathcal{K}_i^{gpp}} q_{i,k}^{gpp} - \sum_{j \in \mathcal{J}_i} q_{i,j} - \sum_{j \in \hat{\mathcal{I}}_i} q_{i,j} + q_i^{ct} = 0, \ i \in \mathcal{I}^G \tag{B.4}$$

$$q_{\hat{i}_{v-1},\hat{i}_v,r} + q_{\hat{i}_v,r}^{gl} = q_{\hat{i}_v,\hat{i}_{v+1},r}, \ \hat{i}_v \in \hat{\mathcal{I}} \tag{B.5}$$

$$\Phi_{i,j} \geq q_{i,j}^2 / C_{i,j}^2 \tag{B.6}$$

$$\Phi_{i,j} \geq p_j^2 - p_i^2 + (\omega_{i,j} + 1)\left((p_i^{min})^2 - (p_j^{max})^2\right) \tag{B.7}$$

$$\Phi_{i,j} \geq p_i^2 - p_j^2 + (\omega_{i,j} - 1)\left((p_i^{max})^2 - (p_j^{min})^2\right) \tag{B.8}$$

$$\Phi_{i,j} \leq p_j^2 - p_i^2 + (\omega_{i,j} + 1)\left((p_i^{max})^2 - (p_j^{min})^2\right) \tag{B.9}$$

$$\Phi_{i,j} \leq p_i^2 - p_j^2 + (\omega_{i,j} - 1)\left((p_i^{min})^2 - (p_j^{max})^2\right) \tag{B.10}$$

$$g_{i,k}^{gpp} = \eta_{i,k}^{gpp} q_{i,k}^{gpp} GCV^{ng}, \ q_{i,k}^{gpp} \geq 0 \tag{B.11}$$

$$g_{i,k}^{ptg} \eta_{i,k}^{el} = q_{i,k}^{ptg} GCV^{ng} \tag{B.12}$$

where the optimization variable $\boldsymbol{u}' = \{p_i, q_{i,k}^{gs}, q_{i,j}, q_i^{ct}, g_{i,k}^{gpp}, \theta_i, g_{i,k}^{gpp}, g_{i,k}^{tpp}, g_{i,k}^{rng}, g_i^{ct}, \omega_{i,j}, \Phi_{i,j}\}$; $g_{i,j}^{ct,max}$ and $q_{i,j}^{ct,max}$ are the upper bounds for electricity and load curtailments; $\Phi_{i,j}$ is an auxiliary variable. The solution of $\omega_{i,j}$ can be obtained as the gas flow direction.

References

[1] UK's gas grid ready for 20% hydrogen blend from 2023: network companies. [Online]. Available: `https://www.spglobal.com/commodityinsights/en/ma` `rket-insights/latest-news/electric-power/011422-uks-gas-grid-ready-f` `or-20-hydrogen-blend-from-2023-network-companies`; 2022-1-12.

[2] Spain's Nortegas to blend green hydrogen. [Online]. Available: `https://www.` `compressortech2.com/news/Spain-s-Nortegas-to-blend-green-hydrogen/`; 2022-5-10.

[3] Briggs T. The combustion and interchangeability of natural gas on domestic burners. Combustion 2014;4(3).

[4] Haeseldonckx D, D'haeseleer W. The use of the natural-gas pipeline infrastructure

for hydrogen transport in a changing market structure. International Journal of Hydrogen Energy 2007;32(10-11):1381–6.

[5] Altfeld K, Pinchbeck D. Admissible hydrogen concentrations in natural gas systems. Gas Energy 2013;2103(03):1–2.

[6] Wang S, Ding Y, Han X, Wang P, Goel L, Ma J. Short-term reliability evaluation of integrated electricity and gas systems considering dynamics of gas flow. IET Generation, Transmission & Distribution 2021;15(20):2857–71.

[7] Cao M, Shao C, Hu B, Xie K, Li W, Peng L, et al. Reliability assessment of integrated energy systems considering emergency dispatch based on dynamic optimal energy flow. IEEE Transactions on Sustainable Energy 2021;13(1):290–301.

[8] Abeysekera M, Wu J, Jenkins N, Rees M. Steady state analysis of gas networks with distributed injection of alternative gas. Applied Energy 2016;164:991–1002.

[9] Clees T, Baldin A, Klaassen B, Nikitina L, Nikitin I, Spelten P. Efficient method for simulation of long-distance gas transport networks with large amounts of hydrogen injection. Energy Conversion and Management 2021;234:113984.

[10] Zhang S, Wang S, Zhang Z, Lyu J, Cheng H, Huang M, et al. Probabilistic multi-energy flow calculation of electricity–gas integrated energy systems with hydrogen injection. IEEE Transactions on Industry Applications 2022;58(2):2740–50.

[11] Zhang Z, Saedi I, Mhanna S, Wu K, Mancarella P. Modelling of gas network transient flows with multiple hydrogen injections and gas composition tracking. International Journal of Hydrogen Energy 2022;47(4):2220–33.

[12] Zhou D, Yan S, Huang D, Shao T, Xiao W, Hao J, et al. Modeling and simulation of the hydrogen blended gas-electricity integrated energy system and influence analysis of hydrogen blending modes. Energy 2022;239:121629.

[13] Cavana M, Mazza A, Chicco G, Leone P. Electrical and gas networks coupling through hydrogen blending under increasing distributed photovoltaic generation. Applied Energy 2021;290:116764.

[14] Cheli L, Guzzo G, Adolfo D, Carcasci C. Steady-state analysis of a natural gas distribution network with hydrogen injection to absorb excess renewable electricity. International Journal of Hydrogen Energy 2021;46(50):25562–77.

[15] Saedi I, Mhanna S, Mancarella P. Integrated electricity and gas system modelling with hydrogen injections and gas composition tracking. Applied Energy 2021;303:117598.

[16] Zhao P, Gu C, Hu Z, Xie D, Hernando-Gil I, Shen Y. Distributionally robust hydrogen optimization with ensured security and multi-energy couplings. IEEE Transactions on Power Systems 2020;36(1):504–13.

[17] Shao C, Feng C, Shahidehpour M, Zhou Q, Wang X, Wang X. Optimal stochastic operation of integrated electric power and renewable energy with vehicle-based hydrogen energy system. IEEE Transactions on Power Systems 2021;36(5):4310–21.

[18] Wu G, Li T, Xu W, Xiang Y, Su Y, Liu J, et al. Chance-constrained energy-reserve co-optimization scheduling of wind-photovoltaic-hydrogen integrated energy systems. International Journal of Hydrogen Energy 2022;.

[19] Mhanna S, Saedi I, Mancarella P, Zhang Z. Coordinated operation of electricity and gas-hydrogen systems with transient gas flow and hydrogen concentration tracking. Electric Power Systems Research 2022;211:108499.

[20] Klimstra J. Interchangeability of gaseous fuels—the importance of the wobbe-index. SAE Transactions 1986;:962–72.

[21] Timashev S, Bushinskaya A. Markov approach to early diagnostics, reliability assessment, residual life and optimal maintenance of pipeline systems. Structural Safety 2015;56:68–79.

[22] Zhou W, Xiang W, Hong H. Sensitivity of system reliability of corroding pipelines to modeling of stochastic growth of corrosion defects. Reliability Engineering & System Safety 2017;167:428–38.

[23] Zhang H, Tian Z. Failure analysis of corroded high-strength pipeline subject to

hydrogen damage based on fem and ga-bp neural network. International Journal of Hydrogen Energy 2022;47(7):4741–58.

[24] Mhanna S, Saedi I, Mancarella P. Iterative lp-based methods for the multiperiod optimal electricity and gas flow problem. IEEE Transactions on Power Systems 2022;37(1):153–66.

[25] Larsen EM, Ding Y, Li YF, Zio E. Definitions of generalized multi-performance weighted multi-state k⁻-out-of-n system and its reliability evaluations. Reliability Engineering & System Safety 2020;199:105876.

[26] Wang S, Ding Y, Ye C, Wan C, Mo Y. Reliability evaluation of integrated electricity–gas system utilizing network equivalent and integrated optimal power flow techniques. Journal of Modern Power Systems and Clean Energy 2019;7(6):1523–35.

[27] Park C, Oh S, Kim C, Choi Y, Ha Y. Effect of natural gas composition and gas interchangeability on performance and emission characteristics in an air–fuel controlled natural gas engine. Fuel 2021;287:119501.

[28] Authority ER. Gas exchangeability in western australia gas—quality specifications of interconnected pipeline system. Western Australia 2007;.

[29] Ennis C, Botros K, Engler D. On the difference between us example supply gases, european limit gases, and their respective interchangeability indices. In: AGA-Operations Conference & Biennial Exhibition. 2009,.

[30] Wang S, Zhai J, Hui H. Optimal energy flow in integrated electricity and gas systems with injection of alternative gas. IEEE Transactions on Sustainable Energy 2023;.

[31] Gas Safety (Management) Regulations. [Online]. Available: `https://www.legislation.gov.uk/uksi/1996/551/introduction/made`; 2022-7-21.

[32] Zhou W. System reliability of corroding pipelines. International Journal of Pressure Vessels and Piping 2010;87(10):587–95.

[33] Zhang S, Zhou W. System reliability of corroding pipelines considering stochastic process-based models for defect growth and internal pressure. International Journal of Pressure Vessels and Piping 2013;111-112:120–30.

[34] Zhang H, Tian Z. Failure analysis of corroded high-strength pipeline subject to hydrogen damage based on fem and ga-bp neural network. International Journal of Hydrogen Energy 2022;47(7):4741–58.

[35] Stephens M, Nessim M. A comprehensive approach to corrosion management based on structural reliability methods. In: International Pipeline Conference; vol. 42622. 2006, p. 695–704.

[36] van Noortwijk J. A survey of the application of gamma processes in maintenance. Reliability Engineering & System Safety 2009;94(1):2–21. Maintenance Modeling and Application.

[37] Ding Y, Cheng L, Zhang Y, Xue Y. Operational reliability evaluation of restructured power systems with wind power penetration utilizing reliability network equivalent and time-sequential simulation approaches. Journal of Modern Power Systems and Clean Energy 2014;2(4):329–40.

[38] Tang Y, Zhao Y, Li W, Xie K, Yu J. Incorporating gas pipeline leakage failure modes in risk evaluation of electricity-gas integrated energy systems. arXiv preprint arXiv:201100776 2020;.

[39] Montiel H, Vıélchez JA, Casal J, Arnaldos J. Mathematical modelling of accidental gas releases. Journal of Hazardous Materials 1998;59(2-3):211–33.

[40] Granger RA. Fluid mechanics. Courier Corporation; 1995.

[41] Soave G. Equilibrium constants from a modified redlich-kwong equation of state. Chemical Engineering Science 1972;27(6):1197–203.

[42] Gholizadeh N, Hosseinian S, Abedi M, Nafisi H, Siano P. Optimal placement of fuses and switches in active distribution networks using value-based minlp. Reliability Engineering & System Safety 2022;217:108075.

[43] Melo A, Pereira M, Leite da Silva A. Frequency and duration calculations in composite generation and transmission reliability evaluation. IEEE Transactions on Power Systems 1992;7(2):469–76.

[44] Grigg C, Wong P, Albrecht P, Allan R, Bhavaraju M, Billinton R, et al. The IEEE reliability test system-1996. A report prepared by the reliability test system task force of the application of probability methods subcommittee. IEEE Transactions on Power Systems 1999;14(3):1010–20.

[45] De Wolf D, Smeers Y. The gas transmission problem solved by an extension of the simplex algorithm. Management Science 2000;46(11):1454–65.

[46] Code for design of oil-gas gathering and transportation systems. [Online]. Available: `https://max.book118.com/html/2019/0407/6013223235002021.shtm`; 2022-9-12.

[47] Github Repositories. [Online]. Available: `https://github.com/ShengWang-E E/Long-Term-Reliability-Evaluation-of-Integrated-Electricity-and-Gas -Systems-with-Alternative-Gas-Inje/tree/main`; 2022-9-11.

[48] Leis B, Stephens D. An Alternative Approach to Assess the Integrity of Corroded Line Pipe - Part I: Current Status. International Ocean and Polar Engineering Conference 1997;05.